preparative column. The active fractions were pooled and lyophilized. Narrow-bore reversed-phase chromatography was performed with each of the active peaks (Fig. 1b). The peak areas were compared with the area of 250 pmol of tomato systemin standard and a 13-amino-acid synthetic tobacco polypeptide standard. The yield of peak Ia was 230 pmol and of peak I was 752 pmol. Peak II yielded 124 pmol. This was the total yield from 50 mg of crude G-25 purified leaf extract.

N-terminal sequencing was performed by Edman chemistry on an Applied Biosystems Model 475 sequencer with pulse liquid update using the manufacturer's protocol. C-terminal sequence analyses were performed on polypeptides digested with carboxypeptidase P and analysed by MALDI mass spectrometry[23]. Samples were prepared for carboxypeptidase P digestion by first treating samples with 1% trifluoroacetic acid at 80 °C for 3 h to hydrolyse the pentose residues from the peptides. The C terminus of peak I was -(K/Q)E, and the N terminus was RGANLPOOSOASSOOSKE. The C terminus of peak II was -DG(K/Q)RP, and the N terminus was NRKPLSOOSOKPADGQ-. A partial N-terminal sequence of peak III determined that the first five N-terminal residues matched the N terminus of the peak II sequence, and the mass was 113 units larger than Tob Sys II. This indicated that a leucine was probably present at its C terminus, as expected from the deduced amino-acid sequence of the preproteins (Fig. 3).

Received 5 December 2000; accepted 30 April 2001.

1. Niall, H. D. The evolution of peptide hormones. *Ann. Rev. Physiol.* **44,** 615–624 (1982).
2. Pearce, G., Strydom, D., Johnson, S. & Ryan, C. A. A polypeptide from tomato leaves induces wound-inducible proteinase inhibitor proteins. *Science* **253,** 895–897 (1991).
3. Matsubayashi, Y. & Sakagami, Y. Phytosulfokine, sulfated peptides that induce the proliferation of single mesophyll cells of *Asparagus officinalis* L. *Proc. Natl Acad. Sci. USA* **93,** 7623–7627 (1996).
4. Fletcher, J. C., Brandu, U., Running, M. P., Simon, R. & Meyerowitz, E. M. Signaling of cell fate decisions by CLAVATA3 in *Arabidopsis* shoot meristems. *Science* **283,** 1911–1914 (1999).
5. Schopfer, C. R., Nasrallah, M. E. & Nasrallah, J. B. The male determinant of self-incompatibility in *Brassica*. *Science* **286,** 1697–1700 (1999).
6. Voet, D. & Voet, J. G. *Biochemistry* 2nd edn 1261 (Wiley and Sons, New York, 1995).
7. Constabel, C. P., Yip, L. & Ryan, C. A. Prosystemin from potato, black nightshade, and bell pepper: primary structures and biological activities of the predicted systemins. *Plant Mol. Biol.* **26,** 55–62 (1998).
8. Pearce, G., Johnson, S. & Ryan, C. A. Purification and characterization from tobacco (*Nicotiana tabacum*) leaves of six small, wound-inducible, proteinase isoinhibitors of the potato inhibitor II family. *Plant Physiol.* **102,** 639–644 (1993).
9. Karban, R. & Baldwin, I. T. *Induced Responses to Herbivory* (Univ. Chicago Press, Chicago, 1997).
10. Meindl, T., Boller, T. & Felix, G. The plant wound hormone systemin binds with the N-terminal part to its receptor but needs the C-terminal part to activate it. *Plant Cell* **10,** 1561–1570 (1998).
11. Schaller, A. & Oecking, C. Modulation of plasma membrane H^+-ATPase activity differentially activates wound and pathogen defense responses in tomato plants. *Plant Cell* **11,** 263–272 (1999).
12. Bryant, J., Green, T., Gurusaddaiah, T. & Ryan, C. A. Proteinase inhibitor II from potatoes: isolation and characterization of its protomer components. *Biochemistry* **15,** 3418–3424 (1976).
13. Ryan, C. A. The systemin signaling pathway: differential activation of plant defensive genes. *Biochim. Biophys. Acta* **1477,** 112–121 (2000).
14. McGurl, B., Pearce, G., Orozco-Cardenas, M. & Ryan, C. A. Structure, expression and antisense inhibition of the systemin precursor gene. *Science* **255,** 1570–1573 (1992).
15. Sommer-Knudsen, J., Bacic, A. & Clarke, A. E. Hydroxyproline-rich plant glycoproteins. *Phytochemistry* **47,** 483–497 (1998).
16. Ferriss, P. J. *et al.* Glycosylated polyproline II rods with kinks as a structural motif in plant hydroxyproline-rich glycoproteins. *Biochemistry* **40,** 2978–2987 (2001).
17. Stratmann, J. W. & Ryan, C. A. Myelin basic protein kinase activity in tomato leaves is induced systemically by wounding and increases in response to systemin and oligosaccharide elicitors. *Proc. Natl Acad. Sci. USA* **94,** 11085–11089 (1997).
18. Scheer, J. M. & Ryan, C. A. A 160 kDa systemin receptor on the surface of *Lycopersicon peruvianium* suspension-cultured cells. *Plant Cell* **11,** 1525–1535 (1999).
19. Matsubayashi, Y. & Sakagami, Y. 120- and 160-kDa receptors for endogenous mitogenic peptide, phyosulfokine-α, in rice plasma membranes. *J. Biol. Chem.* **275,** 15520–15525 (2000).
20. Trotochaud, A. E., Hao, T., Wu, G., Yang, Z. & Clark, S. E. The CLAVATA1 receptor-like kinase requires CLAVATA3 for its assembly into a signaling complex that includes KAPP and a Rho-related protein. *Plant Cell* **11,** 393–405 (1999).
21. Stein, J. C., Howlett, B., Boyes, D. C., Nasrallah, M. E. & Nasrallah, J. B. Molecular cloning of a putative receptor protein kinase gene encoded at the self-incompatibility locus of *Brassica oleraceae*. *Proc. Natl Acad. Sci. USA* **88,** 8816–8820 (1991).
22. Dombrowski, J. E., Gomez, L., Chrispeels, M. & Raikel, N. V. in *Plant Molecular Biology Manual* (eds Gelvin, S. B. & Schilperoort, R. A.) J3, 1–29 (Kluwer Academic, Dordrecht, 1994).
23. Patterson, D. H., Tarr, G. E., Regnier, F. E. & Martin, S. A. C-terminal ladder sequencing via matrix-assisted laser desorption mass spectrometry coupled with carboxypeptidase Y time-dependent and concentration-dependent digestions. *Anal. Chem.* **67,** 3971–3978 (1995).

Supplementary information is available on *Nature*'s World-Wide Web site (http://www.nature.com) or as paper copy from the London editorial office of *Nature*.

Acknowledgements

This research was supported by the College of Agriculture and Home Economics and by the National Science Foundation. We thank S. Vogtman for growing plants; G. Munske for amino-acid sequence analyses; and W. Siems for MALDI mass spectroscopic analyses.

Correspondence and requests for materials should be addressed to C.A.R. (e-mail: cabudryan@hotmail.com). The GenBank accession number for tobacco systemin precursor pro-TobSys-A is AY033148, and for pro-TobSys-B is AY033149.

Structure of a human γδ T-cell antigen receptor

Timothy J. Allison*, Christine C. Winter*, Jean-Jacques Fournié†, Marc Bonneville‡ & David N. Garboczi*

* *Structural Biology Section, Laboratory of Immunogenetics, National Institute of Allergy and Infectious Diseases, 12441 Parklawn Drive, Rockville, Maryland 20852, USA*
† *INSERM U395, CHU Purpan BP3028, 31024 Toulouse, France*
‡ *INSERM U463, Institut de Biologie, 44035 Nantes, France*

T-cell antigen receptors composed of γ and δ polypeptide chains (γδTCRs) can directly recognize antigens in the form of intact proteins or non-peptide compounds, unlike αβTCRs, which recognize antigens bound to major histocompatibility complex molecules (MHC). About 5% of peripheral blood T cells bear γδTCRs, most of which recognize non-peptide phosphorylated antigens[1,2]. Here we describe the 3.1 Å resolution structure of a human γδTCR from a T-cell clone[3] that is phosphoantigen-reactive. The orientation of the variable (V) and constant (C) regions of the γδTCR is unique when compared with αβTCRs or antibodies, and results from an unusually small angle between the Vγ and Cγ domains. The complementarity-determining regions (CDRs) of the V domains exhibit a chemically reasonable binding site for phosphorylated antigens, providing a possible explanation for the canonical usage of the *Vγ9* and *Vδ2* gene segments by phosphoantigen-reactive receptors. Although the γδTCR V domains are similar in overall structure to those of αβTCRs, γδTCR C domains are markedly different. Structural differences in Cγ and Cδ, and in the location of the disulphide bond between them, may enable γδTCRs to form different recognition/signalling complexes than αβTCRs.

γδTCRs, αβTCRs and antibodies are the three types of immune system receptors that are products of rearranging gene segments. Antigen recognition by γδTCRs resembles recognition by antibodies[1,4]. γδ T cells recognize small molecules and intact proteins without the requirement for antigen processing that αβ T cells exhibit[2,5]. Small-molecule recognition by γδ T cells requires cell–cell contact[6,7], suggesting that non-MHC molecules may present small antigens to γδTCRs or that co-stimulation from neighbouring cells is required. Most γδ T cells bear a tissue-specific, restricted set of *V*γ and Vδ domains. For example, 50–90% of human γδ T cells derived from peripheral blood of healthy donors use a combination of *Vγ9* and *Vδ2* gene segments[8]. These γδTCRs are polyclonal with enormous overall sequence diversity at the junctions of their variable, diversity (*D*) and joining (*J*) segments, but with amino-acid similarities at a few junctional positions. *In vitro*, all Vγ9Vδ2$^+$ T cells bearing these sequence similarities can be activated by soluble extracts of *Mycobacteria*, *Plasmodia* and other pathogens[9]. Like most Vγ9Vδ2$^+$ T cells derived from blood, G115 T cells proliferate, secrete lymphokines and lyse target cells in response to stimulation with various natural and synthetic phosphoantigens[3,7,8]. The purified, highly active antigens from *Mycobacteria* are small, phosphate-containing compounds, such as 3-formyl-1-butyl-pyrophosphate[3,10]. Vγ9Vδ2$^+$ T cells are also stimulated by a variety of less active compounds including isopentenyl pyrophosphate[11], alkylamines[12] and aminobisphosphonates[13].

Like αβTCRs and antigen-binding fragments of antibodies (Fabs), the G115 γδTCR is made up of two polypeptide chains each having two immunoglobulin-like domains: an amino-terminal V domain and a carboxy-terminal C domain (Fig. 1a). The Vγ and Vδ domains are each composed of a 'sandwich' of two β-sheets with five inner and four outer strands. The γ-chain and δ-chain CDR

loops at the top of the V domains project out from the receptor (Fig. 1b). The Cγ and Cδ domains are made up of two β-sheets with four inner and three outer strands. The four molecules in the asymmetric unit of the G115 crystal are identical to each other except for small displacements of loops that make contact with neighbouring molecules to form the crystal; the angles between the domains of each receptor are essentially the same.

The G115 γδTCR has a distinctive overall shape compared with αβTCRs and Fabs, in that the C domains of the γδTCR are swung out from under the V domains (Fig. 1). This unusual shape is highlighted by both a small elbow angle and a small Vγ–Cγ inter-domain angle. In antibodies and TCRs, the 'elbow angle' is defined as the angle between the pseudo two-fold symmetry axes that relate V to V and C to C. The elbow angle for G115 is 110° and is smaller than any elbow angle observed in αβTCRs or Fabs (Fig. 2). Analysis of 251 Fab and 11 αβTCR molecules revealed average elbow angles of 159° ($\sigma = 20°$) and 149° ($\sigma = 6°$), respectively, with a range from 125° (Protein Data Bank code 1sbs) to 225° (8fab) for the Fabs and from 140° (1nfd) to 159° (1tcr) for the αβTCRs.

The Vγ–Cγ inter-domain angle of 42°, between the long axis of the Cγ domain and the long axis of the Vγ domain, is markedly smaller than the average angle between the V and C domains of Fabs or αβTCRs (Fig. 1b, γ-chain in gold). The Vδ–Cδ inter-domain angle is 101°. Antibodies and αβTCRs have average angles of 92° (V_L–C_L, $\sigma = 9°$), 76° (V_H–C_H, $\sigma = 11°$), 100° (Vα–Cα, $\sigma = 4°$) and 67° (Vβ–Cβ, $\sigma = 3°$). The smallest angles observed for these molecules are 51°, 50°, 93° and 62° for the light (L), heavy (H), α- and β-chains, respectively. Therefore, the 42° Vγ–Cγ angle of G115 is the smallest inter-domain angle observed among these receptors.

As the relative orientations between Vγ and Vδ and between Cγ and Cδ domains are similar to the relative orientations betweenV–V and between C–C of Fabs and αβTCRs, the small angle between the Vγ and Cγ domains shifts both Cγ and Cδ to one side (Fig. 1b). The G115 γδTCR exhibits 1,077 Å^2 of buried surface in the interface between its V and C domains, similar to that for Fabs and αβTCRs, which average about 900 Å^2 and 1,200 Å^2, respectively. Although the correlation between the amount of buried surface in a V–C interface and the elbow angle is not known, it is expected that the residues in this interface affect the elbow angle. As the residues found in the G115 interface are conserved in most human and mouse γ-chain and δ-chain genes, it is likely that other γδTCRs will have similar elbow angles and a comparable molecular shape.

Sequence similarities between Vγ and Vβ and between Vδ and Vα domains clearly indicate their relatedness, but whether Vγ or Vδ is more like an antibody V_L or V_H domain is more difficult to determine. Both possible superpositions of Vγ and Vδ with V_L or V_H domains yield similar root-mean-square (r.m.s.) deviations in α-carbon positions and do not distinguish which V domain is more like a V_L or a V_H domain. On the basis of elbow angle considerations, we chose to structurally align Vγ with V_H and Vδ with V_L. This yields an elbow angle of 110° for G115 and an angle that is less than 180° for most Fabs and for all structurally determined TCRs (Fig. 2). Alignment in this way of the γδTCR domains with their analogous domains in αβTCRs and in Fabs shows the overall similarity of these immunoglobulin-like domains and highlights their differences (see Fig. 1 of Supplementary Information).

The CDR loops of γδTCRs, αβTCRs and antibodies comprise the sites of antigen recognition. The loop residues of G115 are: γ25–36, δ25–35 in CDR1 loops; γ53–59, δ51–55 in CDR2 loops; γ73–79, δ69–74 in hypervariable-4 loops (HV4s); and γ99–111, δ94–108 in CDR3 loops. The CDR1, CDR2 and HV4 loops of Vγ are similar in length and in relative position to those of Vβ. The CDR1 and HV4 loops of Vδ are also similar to those of Vα. However, the CDR2 loop of Vδ differs in relative position with that of Vα, in which the C″ strand pairs with the D strand of the outer β-sheet. In Vδ, as in Vγ, Vβ, V_L and V_H, the C″ strand is paired with the C′ strand of the inner β-sheet of the domain. This C″–C′ pairing in Vδ has been seen in the structure of an isolated human Vδ3 domain[14].

As expected, the Vδ2 domain of the G115 structure is very similar to the isolated Vδ3 domain[14]; the r.m.s. difference between the two domains is 1.2 Å over 86 α-carbon atoms. There are two significant differences between Vδ2 and Vδ3 domains. The CDR2 (C′–C″) loop of Vδ2 (and Vδ1) is three residues shorter than the equivalent loop in Vδ3. Unlike the solvent-exposed CDR1 loop of Vδ3, the CDR1 loop of Vδ2 contains an isoleucine that tucks into the core of the domain and holds the loop away from CDR3. As the CDR1 loop

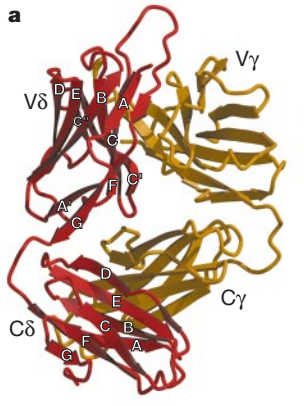

Figure 1 Views of the G115 Vγ9Vδ2 TCR. **a**, View of Vδ and Cδ (red) and Vγ and Cγ (gold) domains. CDR loops are at the top. **b**, View after a 90° rotation around the vertical axis. The nine β-strands of the V domains are labelled A–G, including A′, C′, and C″. The seven β-strands of the C domains are labelled A–G. In each domain, strands A, B, E, and D form one β-sheet, and strands G, F and C (including A′, C′ and C″ in the V domains) form the other sheet. The Vγ–Vδ interface involves the A′GFCC′C″ β-sheets. The Cγ–Cδ interface involves the ABED β-sheets.

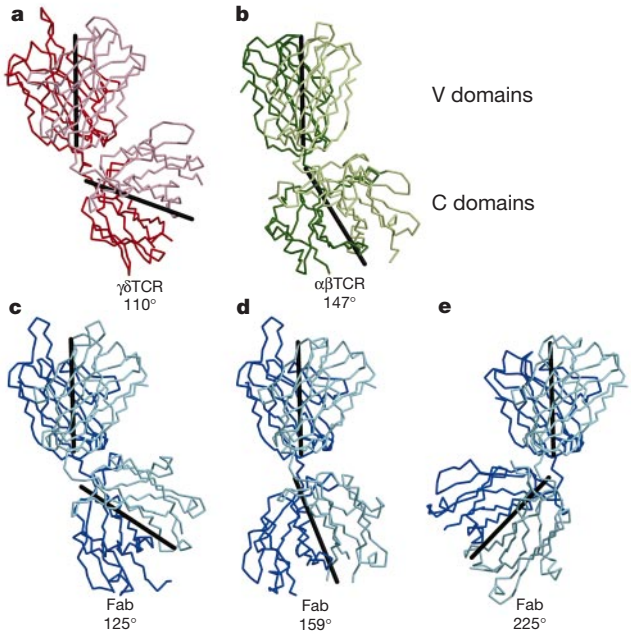

Figure 2 Overall structure of a γδTCR, αβTCR and Fabs. **a**, γδTCR G115 (red); **b**, αβTCR (green); and **c–e**, three Fabs (blue) aligned using both V domains. Note the atypical position of the γδ C domains. The pseudo two-fold symmetry axes (dyads) within the V and C domains are shown (solid lines). The elbow angle between these axes is listed for each representative molecule (αβTCR: Protein Data Bank code 1qsf; Fabs: **c**, 1sbs; **d**, 1hil; **e**, 8fab). The γ-, β- and H chains and the δ-, α- and L chains are in lighter and darker shades, respectively.

of Vδ1 contains a tryptophan residue at this position, its loop may more closely resemble that of Vδ2 than Vδ3.

The CDR-containing surface of the G115 V domains exhibits more protrusions and clefts compared with the flatter surfaces of αβTCRs that bind a peptide–MHC complex, and of antibodies that bind protein antigens (Fig. 3). The jagged surface of this γδTCR resembles the surface of an antibody that binds a small-molecule antigen. If phosphoantigens are recognized while bound to other molecules, the shape of presentation molecules that would complement this rather rough γδTCR surface would probably be different from the shape of MHC molecules.

Vγ9-bearing T cells respond to the superantigen staphylococcal enterotoxin A (SEA)[15]. Superantigens bind to αβTCRs through the side and top of the Vβ domain; in particular the CDR2β and HV4β loops and nearby framework regions[16]. The structural similarity of Vγ9 and Vβ and the superposition of Vγ9 and SEA with Vβ and staphylococcal enterotoxin B (SEB) of the Vβ–SEB complex suggests that the interaction of Vγ with SEA will resemble that of Vβ with SEB[16], in agreement with a recent report[17].

From the sequences of many TCRs, it has been noted that CDR3γ loops are similar in length to CDR3β loops, and that CDR3δ loops are longer than CDR3α loops[4]. For G115, however, both of its CDR3 loops are similar in length to those of αβTCRs for which the structures have been determined. Unlike αβTCRs, the G115 CDR3 loops protrude significantly from the rest of the molecule and create a cleft between them. Portions of CDR1δ, CDR1γ and CDR2γ combine with the cleft between the CDR3 loops to form a pocket in G115 that is likely to be the phosphoantigen-binding site. In the packing of the crystal, the CDR3δ loop of each molecule makes a contact with Arg γ59 of a crystallographically related molecule that may partially block the cleft and may be responsible for preventing phosphoantigen binding in our crystal-soaking and co-crystallization experiments.

Phosphoantigen molecules are composed of pyrophosphate, a short alkyl carbon chain, and often a chemically reactive group. G115 γδ T cells respond to the *Mycobacterium tuberculosis* antigen 3-formyl-1-butyl-pyrophosphate, which has a pyrophosphate, an alkyl chain and a formyl group that are important for T-cell activation (Fig. 3b)[11,18]. In cellular assays, excess pyrophosphate inhibits activation by phosphoantigens[18]. The possible phosphoantigen-binding site on G115 is the positively charged pocket formed by Arg 59 of CDR2γ, Lys 109 of CDR3γ, and Arg 51 of CDR2δ, which may interact with the phosphates of the antigen (Fig. 3c, d). Similar positively charged pockets are found in antibodies that bind phosphate-containing antigens.

A key residue of the putative binding site is Lys 109 of the CDR3γ loop, which derives from the *JγP* gene segment. In the approximately 50 reported sequences of receptors from γδ T cells activated by phosphoantigens, all use the *Vγ9* gene segment and almost all use the *JγP* gene segment[19,20]. A few reactive clones use the *Jγ1* or *Jγ2* gene segments that encode a lysine residue in a similar position in the CDR3 sequence that may serve the same role as Lys γ109 of JγP. The other *Jγ* gene segments that have not been found in reactive clones, *JγP1* and *JγP2*, do not encode an analogous lysine residue. Of the Vγ-encoded residues that are located near the putative binding pocket, all but two (Thr γ33, Trp γ100) of them are found only in the *Vγ9* gene segment (Fig. 3d); this may explain the absolute requirement for Vγ9 in phosphoantigen-reactive clones.

The CDR3 loops link the ends of the F and G β-strands in all V domains. In Vγ9 of G115, the two-stranded FG β-sheet extends two residues farther than known F and G strands in Vβ domains. Only four residues at the end of the 13-residue CDR3γ loop are not in regular β-sheet structure. About one-third of the phosphoantigen-reactive sequences have no N-encoded residues at the Vγ9–JγP joint, and the others have from one to three N-encoded residues, with G115 having two[8,19].

CDR3δ sequences in γδTCRs are, in general, very diverse as up to three *D* gene segments with N-addition can be used[1]. CDR3δ chains from phosphoantigen-reactive γδTCRs usually bear a single *Dδ3* gene segment but can have from three to twelve residues of diverse sequence encoded by *D*- and N-derived nucleotides[8]. The CDR3δ loop of G115 consists of fifteen residues, seven from *D* and N additions, three from *Vδ2* and five from *Jδ1*. All phosphoantigen-reactive clones have a conserved hydrophobic residue, encoded by N-addition nucleotides, at position 97 of CDR3δ[19] with Leu, Ile, Val and Gly being predominant; G115 has a Leu at δ97 (Fig. 3d). This conserved hydrophobe may interact with hydrophobic parts of

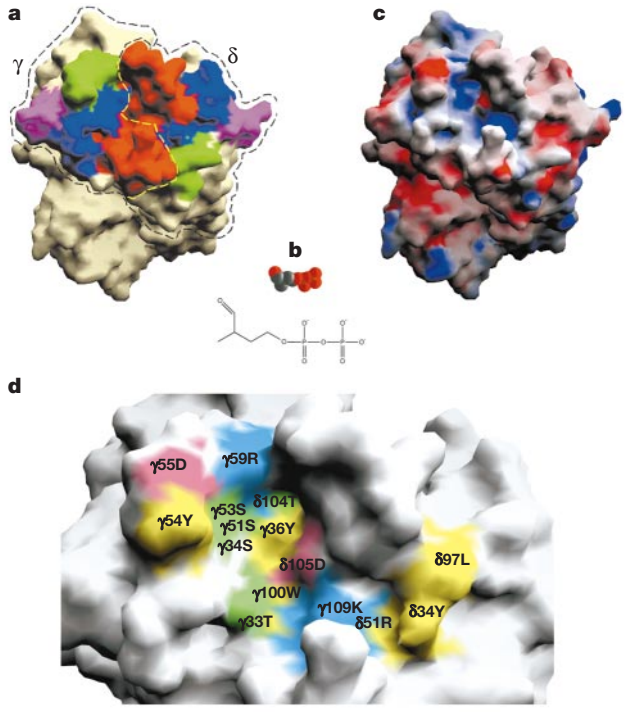

Figure 3 Surface representations of G115. **a**, The surface of G115 is coloured by CDR loops (CDR1, blue; CDR2, green; HV4, pink; and CDR3, red). **b**, 3-formyl-1-butyl-pyrophosphate is shown as a drawing and as a space-filling model (at the same scale as G115 in **a** and **c**). **c**, The surface potential of G115 is colour-coded from red (–10 kT) to blue (+10 kT). The top of the molecule, containing the CDR loops, is facing the viewer. The cleft between the two CDR3 loops contains positively charged patches (blue), which line the phosphoantigen-binding site. **d**, Enlarged view of the cleft shows the location of charged (negative in red; positive in blue), hydrophobic (yellow) and polar (green) residues.

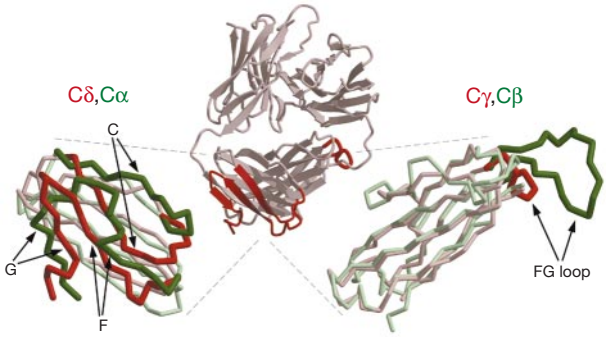

Figure 4 Comparison of the γδTCR and αβTCR C domains. Superpositions of Cδ with Cα (left) and Cγ with Cβ (right) are shown. Differences between the domains are highlighted; the locations of these differences within the G115 structure are also shown. Cδ and Cγ are shown in red. Cα and Cβ from 1qsf are shown in green. The outer face of Cδ contains β-strands C, F and G, which form a regular β-sheet. Cγ has a much shorter FG loop.

phosphoantigen molecules and seems to be antigen-selected, as thymic Vγ9Vδ2 TCR sequences are not restricted to being hydrophobic at δ97 (ref. 19). Of the δ-chain residues that form the binding pocket, only Tyr 34 of CDR1δ and Arg 51 of CDR2δ are part of the *Vδ2* gene segment (Fig. 3d). Both of these residues are also found in *Vδ1*. The other residues in the putative binding site derive from *Jδ1* or *Dδ3* gene segments, or are N-encoded. An unusual feature of the Vδ2 domain is an unpaired and almost entirely buried cysteine residue that is located at the base of the CDR3 loop and is not present in other human or murine *Vδ* gene sequences. The putative antigen-binding site described here may explain the broad antigen reactivity by polyclonal populations of $V\gamma9V\delta2^+$ T cells, as most residues that seem necessary for phosphoantigen recognition are encoded by either *V* or *J* gene segments.

Like αβTCRs, a functional γδ receptor at the T-cell surface is a complex of the TCR chains and the CD3γ, -δ, -ϵ and -ζ subunits, which associate with cytoplasmic proteins for T-cell signalling. The extracellular portions of the CD3γ, -δ and -ϵ subunits contain a single immunoglobulin-like domain and may interact with the C domains of the TCR. To discern how CD3 interacts with both γδ- and αβTCRs, we looked for a conserved surface to which CD3 may bind. Examination of both the shape and nature of the surfaces of CαCβ and CγCδ revealed no clear similarities. Furthermore, there are only a few solvent-exposed residues that are structurally conserved in both Cβ and Cγ domains. Residues Lys γ186 and Tyr γ191 flank the DE loop on both sides and are near, but not involved with, the Vγ–Cγ interface. Residue Arg γ209, on the opposite side of the Cγ domain in the middle of strand F, is surrounded by other charged residues (Glu γ207, Lys γ171, Lys γ172) that are not found in Cβ. We also compared the location of N-linked glycosylation sites between the C domains. Although the position of the single glycosylation site in Cγ is structurally equivalent to the single site in human Cβ, only one (Asn δ134) of the two sites in Cδ can be regarded as spatially equivalent to one (Asn α183) of the three glycosylation sites in Cα. From this comparison of TCRs, it is not possible to conclude where or how the extracellular domains of CD3 subunits may interact with the extracellular portions of TCRs.

The C domains of the γδTCR are structurally different from those of αβTCRs. First, although sequence alignments predicted that the Cγ domain would have a long, Cβ-like FG loop[21], the structure of G115 reveals Cγ to have a much shorter FG loop (Fig. 4, in red at right; see also Fig. 2 of Supplementary Information. The Cγ FG loop is seven residues in length and is tucked in close to the core of the Cγ domain, whereas the Cβ FG loop is 19 residues in length and extends away from the core of Cβ. As the human and murine Cγ sequences have 76% sequence identity in their FG loops and F and G strands, the murine Cγ domain will probably also possess a short FG loop. The FG loop of Cβ has been proposed to be part of the binding site for the CD3ϵ subunit[22]. The much smaller Cγ loop suggests that, if CD3ϵ binds to Cγ, the FG loop of Cγ is not the primary site of CD3ϵ interaction. The second difference between the C domains of γδ and αβTCRs is that the secondary structure of Cδ is unlike that of Cα. Cδ is composed of a regular immunoglobulin-like domain with a regular three-stranded *β*-sheet as its outer face; Cα contains unusual secondary structure instead of a regular outer *β*-sheet (Fig. 4, in green at left). Clearly, when compared to the αβTCR C domains, the C domains of γδTCRs will present different molecular surfaces to CD3 subunits and to other cell-surface molecules. This could allow one kind of signalling complex to form with γδTCRs and a different kind to form with αβTCRs.

The two kinds of TCRs differ in the number of residues between the end of the C domains and in the position of the interchain disulphide bond. In αβTCR structures, the last ordered residues of Cα and Cβ are 6 or 7 residues and 1 or 2 residues, respectively, away from the interchain disulphide. In G115, the electron density indicates that δ206 and γ230 are the last ordered residues, although the δ- and γ-chains that are in the crystals are longer and end at residues δ229 and γ242, just before the interchain disulphide cysteines. Thus, there are 23 and 12 residues of the δ-chain and γ-chain, respectively, between the end of the C domains and the interchain disulphide. The number of residues between the interchain disulphide and the transmembrane domain is almost the same in both γδTCRs and αβTCRs. Other γδTCRs that use the *Cγ2* gene segment lack an interchain disulphide, and alternative splicing of additional *Cγ2* exons can result in an even longer span between the end of the Cγ domain and the membrane. The longer protein chain between the γδ C domains and the interchain disulphide may provide an additional means of making γδTCRs distinct by means of the altered association of CD3 subunits or by a greater flexibility on the membrane of a γδ receptor.

Structural differences between γδTCRs and αβTCRs both in overall shape and in the C domains suggest a specific role for γδTCRs in immunity and point to those same regions in αβTCRs as being important for αβTCR function. The germline-encoded phosphoantigen-binding site described here may account for the broad antigen reactivity of polyclonal, peripheral blood $\gamma\delta^+$ T cells that can be activated simultaneously by similar ligands, producing a significant effect on the immune system. □

Methods

Crystallization

The G115 (ref. 3) (or G9 (refs 8, 19, 23)) γ- and δ-chains (Vγ9JPC1 and Vδ2D3J1C, see http://imgt.cines.fr) were expressed as insoluble proteins in *Escherichia coli* with and without selenomethionine, then refolded together by rapid dilution in 1 l of 1 M L-arginine, 0.1 M Tris-HCl, pH 8.0 and 0.2 mM reduced/0.2 mM oxidized glutathione. After dialysis against 10 mM Tris-HCl pH 8.0, concentration by cation exchange chromatography at pH 5.5, and purification by size exclusion chromatography at pH 8.0, the refolded protein formed crystals in hanging drops containing 4 mg ml^{-1} protein, 28% polyethylene glycol 4000, 0.2 M Li_2SO_4, 0.1 M Tris-HCl, pH 8.5 and 20% glycerol.

Structure determination

X-ray data were measured at three wavelengths on a selenomethionine-containing crystal at beamline X9B of the National Synchrotron Light Source (Brookhaven National Laboratory) and at the CuKα wavelength (525° of data) on a crystal soaked in the synthetic phosphoantigen bromohydrin pyrophosphate (BrHPP)[18]. Data were integrated and scaled with HKL2000 (ref. 24). We located selenium atoms (12 out of 28) using SnB[25]. Refinement of selenium positions and calculation of experimental phases were performed with SHARP[26]; values of f″ were each refined as single-wavelength anomalous diffraction calculations, followed by f′ refinement as a multiwavelength anomalous diffraction (MAD) calculation. Four sets of selenium atoms (20 total) exhibited non-crystallographic symmetry (NCS). Density modification, performed with DM from the CCP4 suite[27], confirmed that there were four γδTCR molecules present in the asymmetric unit. Iterative cycles of NCS averaging, reciprocal space phase combination, and other crystallographic calculations were performed with the RAVE[28] and CCP4 (ref. 27) program packages. Crystallographic statistics are presented in Supplementary Information.

The G115 model was built using O (ref. 29) and refined against the MAD data using the maximum likelihood Hendrickson–Lattman (MLHL) target in CNS[30]. The nearly complete model was refined against the higher resolution data from the antigen-soaked native crystal using the maximum likelihood amplitude (MLF) target in CNS. Small crystals (< 100 μm) and high redundancy contributed to poor merging statistics; however, intensities for the highest bin of resolution were well over 2σ and R_{free} for the highest resolution bin was less than 40% for the final model. Therefore, all data to 3.12 Å were included in refinement. The anomalous signal of these data (with model phases) was able to confirm the locations of sulphur atoms at cysteines, methionines and two sulphates involved in a crystal contact, but did not reveal any sites that could be attributed to the brominated antigen. Furthermore, the presence of the antigen could not be confirmed from the electron density map. Tight NCS restraints were applied during initial model refinement, but were later relaxed to 200 kcal mol^{-1} $Å^{-2}$ for main-chain atoms and 100 kcal mol^{-1} $Å^{-2}$ for side-chain atoms. Each of the four domains of the TCR was restrained by a separate NCS operator, thus allowing the movement of domains relative to each other. The r.m.s. deviations between equivalent domains are less than 0.05 Å and 0.09 Å for main-chain and side-chain atoms, respectively. NCS restraints were not applied to the CDRs, switch regions and loops that exhibited modest conformational variation between molecules.

R_{free} was monitored throughout refinement using reflections (5% of total) that were selected in 35 resolution shells. Water molecules were picked using the water_pick and water_delete scripts in CNS into locations that exhibited 3.5σ density in an F_o–F_c map; 1.3σ density in a $2F_o$–F_c map; 1σ density in a simulated anneal $2F_o$–F_c composite omit map; and proper hydrogen-bonding distance and geometry and that were visually confirmed in the program O. The final model (R = 21.9% and R_{free} = 26.6%) includes four copies of residues δ1–206 and γ1–230, plus 54 water molecules and 2 sulphates in the asymmetric unit. A Ramachandran plot of the model shows 81% of residues in the most favoured regions and 17% in additionally allowed regions, with no residues in disallowed

regions. Amino-acid side chains exhibiting weak electron density were built with steric and geometric constraints. We generated the figures with GRASP, Molscript and Raster3D.

Structural comparisons

We carried out structural comparisons against 251 Fab and 11 αβTCR models. Superpositions were performed using LSQMAN[28]. The inter-domain, intra-chain angles (for instance Vγ–Cγ) were calculated as the supplement of the rotation angle necessary for superposition of the conserved α-carbon atoms of the B and F strands of each domain. Because the Vγ–Vδ interface involves the A′GFCC′C″ β-sheet whereas the Cγ–Cδ interface involves the ABED β-sheet (Fig. 1), V domain strands B and F were explicitly superimposed onto C domain strands F and B. The elbow angle between the V and C domains was calculated as the angle between the pseudo-dyads, described by direction cosines, which result from a superposition of V or C domains. Buried interfaces were calculated with CNS using a probe radius of 1.4 Å. Structures of αβTCRs and Fabs are referred to by their Protein Data Bank identification codes (http://www.rcsb.org).

Received 16 January; accepted 30 April 2001.

1. Hayday, A. C. γδ cells: a right time and a right place for a conserved third way of protection. *Annu. Rev. Immunol.* **18,** 975–1026 (2000).
2. Chien, Y. H., Jores, R. & Crowley, M. P. Recognition by γ/δ T cells. *Annu. Rev. Immunol.* **14,** 511–532 (1996).
3. Constant, P. *et al.* Stimulation of human γδ T cells by nonpeptidic mycobacterial ligands. *Science* **264,** 267–270 (1994).
4. Rock, E. P., Sibbald, P. R., Davis, M. M. & Chien, Y. H. CDR3 length in antigen-specific immune receptors. *J. Exp. Med.* **179,** 323–328 (1994).
5. Sciammas, R. *et al.* Unique antigen recognition by a herpesvirus-specific TCR-γδ cell. *J. Immunol.* **152,** 5392–5397 (1994).
6. Morita, C. T. *et al.* Direct presentation of nonpeptide prenyl pyrophosphate antigens to human γδ T cells. *Immunity* **3,** 495–507 (1995).
7. Lang, F. *et al.* Early activation of human Vγ9Vδ2 T cell broad cytotoxicity and TNF production by nonpeptidic mycobacterial ligands. *J. Immunol.* **154,** 5986–5994 (1995).
8. Davodeau, F. *et al.* Close correlation between Daudi and mycobacterial antigen recognition by human γδ T cells and expression of V9JPC1γ/V2DJCδ-encoded T cell receptors. *J. Immunol.* **151,** 1214–1223 (1993).
9. Fournié, J. J. & Bonneville, M. Stimulation of γδ T cells by phosphoantigens. *Res. Immunol.* **147,** 338–347 (1996).
10. Belmant, C. *et al.* 3-formyl-1-butyl pyrophosphate: a novel mycobacterial metabolite-activating human γδ T cells. *J. Biol. Chem.* **274,** 32079–32084 (1999).
11. Tanaka, Y., Morita, C. T., Nieves, E., Brenner, M. B. & Bloom, B. R. Natural and synthetic non-peptide antigens recognized by human γδ T cells. *Nature* **375,** 155–158 (1995).
12. Bukowski, J. F., Morita, C. T. & Brenner, M. B. Human γδ T cells recognize alkylamines derived from microbes, edible plants, and tea: implications for innate immunity. *Immunity* **11,** 57–65 (1999).
13. Kunzmann, V. *et al.* Stimulation of γδ T cells by aminobisphosphonates and induction of antiplasma cell activity in multiple myeloma. *Blood* **96,** 384–392 (2000).
14. Li, H. *et al.* Structure of the Vδ domain of a human γδ T-cell antigen receptor. *Nature* **391,** 502–506 (1998).
15. Loh, E. Y. *et al.* Gene transfer studies of T cell receptor-γδ recognition. Specificity for staphylococcal enterotoxin A is conveyed by Vγ9 alone. *J. Immunol.* **152,** 3324–3332 (1994).
16. Li, H. *et al.* Three-dimensional structure of the complex between a T cell receptor β chain and the superantigen staphylococcal enterotoxin B. *Immunity* **9,** 807–816 (1998).
17. Morita, C. T. *et al.* Superantigen recognition by γδ T Cells: SEA recognition site for human Vγ2 T cell receptors. *Immunity* **14,** 331–344 (2001).
18. Belmant, C. *et al.* A chemical basis for selective recognition of nonpeptide antigens by human γδ T cells. *FASEB J.* **14,** 1669–1670 (2000).
19. Davodeau, F. *et al.* Peripheral selection of antigen receptor junctional features in a major human γδ subset. *Eur. J. Immunol.* **23,** 804–808 (1993).
20. Panchamoorthy, G. *et al.* A predominance of the T cell receptor Vγ2/Vδ2 subset in human mycobacteria-responsive T cells suggests germline gene encoded recognition. *J. Immunol.* **147,** 3360–3369 (1991).
21. Bentley, G. A., Boulot, G., Karjalainen, K. & Mariuzza, R. A. Crystal structure of the β chain of a T cell antigen receptor. *Science* **267,** 1984–1987 (1995).
22. Wang, J. *et al.* Atomic structure of an αβ T cell receptor (TCR) heterodimer in complex with an anti-TCR Fab fragment derived from a mitogenic antibody. *EMBO J.* **17,** 10–26 (1998).
23. Davodeau, F. *et al.* Secretion of disulfide-linked human T-cell receptor γδ heterodimers. *J. Biol. Chem.* **268,** 15455–15460 (1993).
24. Otwinowski, Z. & Minor, W. Processing of X-ray diffraction data collected in oscillation mode. *Methods Enzymol.* **276,** 307–326 (1997).
25. Smith, G. D., Nagar, B., Rini, J. M., Hauptman, H. A. & Blessing, R. H. The use of SnB to determine an anomalous scattering substructure. *Acta Crystallogr. D* **54,** 799–804 (1998).
26. de la Fortelle, E. & Bricogne, G. Maximum-likelihood heavy-atom parameter refinement for multiple isomorphous replacement and multiwavelength anomalous diffraction methods. *Methods Enzymol.* **276,** 472–494 (1997).
27. Bailey, S. The CCP4 suite—programs for protein crystallography. *Acta Crystallogr D* **50,** 760–763 (1994).
28. Kleywegt, G. J. & Jones, T. A. in *From First Map to Final Model* (eds. Bailey, S., Hubbard, R. & Waller, D.) 59–66 (SERC Daresbury Laboratory, Warrington, 1994).
29. Jones, T. A., Zou, J. Y., Cowan, S. W. & Kjeldgaard, M. Improved methods for binding protein models in electron density maps and the location of errors in these models. *Acta Crystallogr. A* **47,** 110–119 (1991).
30. Brünger, A. T. *et al.* Crystallography & NMR system: A new software suite for macromolecular structure determination. *Acta Crystallogr. D* **54,** 905–921 (1998).

Supplementary information is available on *Nature's* World-Wide Web site (http://www.nature.com) or as paper copy from the London editorial office of *Nature*.

Acknowledgements

We thank C. Hammer for mass spectrometry; M. Garfield for amino-acid sequencing; S. Garman for advice and discussions; and Z. Dauter and K. R. Rajashankar for help at beamline X9B at the National Synchrotron Light Source at Brookhaven National Laboratory, which is supported by the US Department of Energy, Division of Materials Sciences and Division of Chemical Sciences. T.J.A. is supported by a postdoctoral fellowship from the Cancer Research Institute. This work is supported by the intramural program of the National Institute of Allergy and Infectious Diseases.

Correspondence and requests for materials should be addressed to T.J.A. (e-mail: tallison@niaid.nih.gov) or D.N.G. (e-mail: garboczi@nih.gov).
Coordinates have been deposited at the Protein Data Bank (identification code 1hxm) and will be released on publication.

corrections

Plant diversity enhances ecosystem responses to elevated CO_2 and nitrogen deposition

Peter B. Reich, Jean Knops, David Tilman, Joseph Craine, David Ellsworth, Mark Tjoelker, Tali Lee, David Wedin, Shahid Naeem, Dan Bahauddin, George Hendrey, Shibu Jose, Keith Wrage, Jenny Goth & Wendy Bengston

Nature **410,** 809–812 (2001).

This paper should have included the following acknowledgement:

We thank the US Department of Energy for financial support, with additional support from the US National Science Foundation Long-Term Ecological Research Program. □

Enabling the chemistry of life

C. Walsh

Nature **409,** 226–231 (2001).

In Fig. 4 of this *Insight* article, the P450 haem active site is wrongly shown as a uroporphyrinogen I rather than a protoporphyrin IX macrocycle. The correct version of the molecule is shown here. □